Rev. Roum. Sci. Techn.– Électrotechn. et Énerg.
Vol. **69**, *2*, pp. 123–128, Bucarest, 2024

COMPARATIVE STUDY OF INNER AND OUTER ROTOR FLUX REVERSAL PERMANENT MAGNET MACHINE FOR DIRECT DRIVE WIND TURBINE

AHCENE BOULAYOUNE[1,2], ADEL OUBELAID[3], AREZKI CHIBAH[4]

Keywords: Flux reversal machine; Outer rotor; Inner rotor; Direct drive; Wind turbine; Particle swarm optimization; Computer-aided design.

The topology, operation principle, and electromagnetic performance of the inner rotor flux reversal permanent magnet (IRFRPM) machine and the outer rotor flux reversal permanent magnet (ORFRPM) machine are quantitatively compared in this paper. First, the mass torque of both machines is optimized and compared using particle swarm optimization (PSO) combined with the finite element method (FEM). Second, the static properties of both machines are calculated using finite element analysis (FEA). Both machines are suitable for direct-drive wind turbines, but ORFRPM outperforms IRFRPM.

1. INTRODUCTION

Wind systems are increasingly improved and reduced. On the generator side, it demands compact and lightweight to place on the pylon and coupled directly to the wind turbine. These advantages are seen over a high-speed conventional generator where the coupling must be done through a gearbox, which generates installation and maintenance costs, a complex control, slow response to fluctuations in wind and changes in expenses, etc. However, the generator's rotational speed must be low to match the wind turbine's speed and produce electricity similar to the main frequency (50-60 Hz). According to electrical machine design principles, using conventional structures (induction machine, synchronous machine ...) requires many poles in the stator and rotor and complex winding. Potentially, the toothed plots permanent magnet (PM) machines, namely flux reversal (FR), doubly salient (DS), and flux switching (FS), offer simple structures, robust and high working efficiency because the coil is concentric, and there is no coil or magnet in the rotor. Flux reversal machines (FRM) used for high-speed drive applications were initially discussed in [1] and for low-speed applications in [2]. After that, FRM research focused on design aspects [3]. Furthermore, authors have explored the design intricacies of flux reversal machines, such as the three-phase flux reversal machine (FRM) [4,5], which showcases a doubly salient stator-permanent magnet configuration. These machines, characterized by a simple reluctance rotor, stator with armature windings, and permanent magnets, have shown high effectiveness in various applications. By exploring the design nuances of flux reversal machines, researchers aim to enhance their efficiency, performance, and applicability across different domains within the realm of electrical machinery [6–9]. These internal rotors are important in wind turbine applications [10–13]. An outer rotor flux reversal machine was proposed in [14] for rooftop wind power generation. This low-speed machine has six stator plots with two permanent magnet pairs on each stator plot. This machine is designed for 214 rpm, 2.4 kW. This paper proposes the outer rotor flux reversal permanent magnet machine (ORFRPM) for a direct drive wind turbine. It has 12 stator plots with four PM pairs on each stator plot and 64 rotor teeth. The proposed ORFRPM machine is quantitatively compared with his equivalent IRFRPM machine in terms of mass torque, Fig. 1, optimized by using PSO combined with FEM.

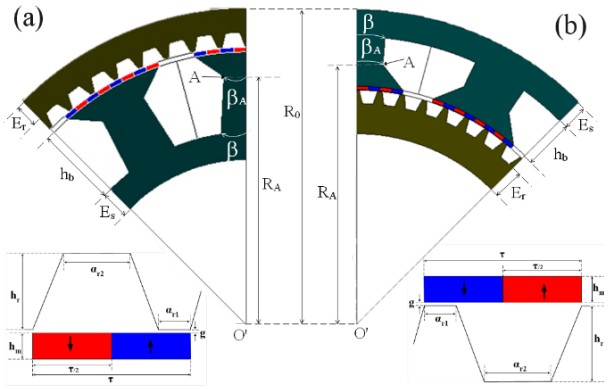

Fig. 1 – Teeth, permanent magnets and global parameters: ORFRPM (a) and IRFRPM (b).

The static characteristics are evaluated with FEM, compared and discussed, and finally, conclusions are drawn.

2. PARTICLE SWARM OPTIMIZATION (PSO)

The PSO algorithm is similar to the genetic algorithm in the population-based research method and searches for the optimal solution by updating the generations, but their strategies are different. In the population, also called "swarm", each individual or particle has a position $x(t)$ and a speed v(t) dynamically adjusted, relative to the proper experience of the particle (cognitive component: p-$x(t)$), as well as to those of neighboring particles (social component: g-$x(t)$), as shown in Fig. 2.

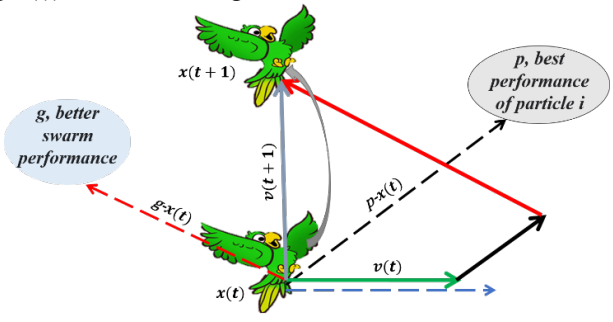

Fig. 2 – PSO basic philosophy.

[1] Research Laboratory in Electronic Systems and Electrical Systems Engineering, Military Academy of Cherchell-Tipaza, Algeria.
[2] Université de Bejaia, Laboratoire de Génie Electrique de Bejaia, Targa Ouzemour, 06000 Bejaia, Algeria.
[3] Université de Bejaia, Faculté de Technologie, Laboratoire de Technologie Industrielle et de l'Information, Targa Ouzemour, 06000, Bejaia, Algeria
[4] Laboratoire des systèmes électriques et industriels (LSEI), Université des Sciences et de la Technologie Houari Boumediene, Alger, Algeria
E-mails: ahcene.boulayoune@univ-bejaia.dz, adel.oubelaid@univ-bejaia.dz, achibah@usthb.dz

DOI: 10.59277/RRST-EE.2024.69.2.1

Various versions of the method generally dealing with the influence of parameters on the algorithm's convergence, have been proposed in the literature [15–18]. Among them, our choice fell on that described in [16], where the algorithm is more stable, and the convergence is more secure than previous versions. At the start of the algorithm, each particle is positioned randomly in the problem's search space. During each iteration, each particle is updated according to three components: its current speed $v(t)$, its best solution p, and the best solution obtained in its vicinity g. This gives the equation the following movement:

$$v(t+1) =$$

$$= \chi \times \Big(v(t) + C_1 \times \big(p - x(t)\big) + C_2 \times \big(g - x(t)\big)\Big), \quad (1)$$

$$x(t+1) = x(t) + v(t+1), \quad (2)$$

with $x(t)$: the current position, χ: constriction coefficient

$$\chi = \frac{2}{\varphi - 2 + \sqrt{\varphi^2 - 4\times\varphi}}, \quad (3)$$

and with φ a confidence coefficient, φ = 4.1, and C_1, C_2 acceleration coefficients.

$$C_1 = \left(\frac{\varphi}{2}\right) * \text{random}(0,1)), \quad (4)$$

$$C_2 = \left(\frac{\varphi}{2}\right) * \text{random}(0,1). \quad (5)$$

PSO is a population algorithm. It starts with a random initialization of the swarm in the research space. At each iteration of the algorithm, each particle is moved following (1) and (2). Once the particles are performed, the new positions are evaluated. The p and g are then updated. This procedure is summarized by the following pseudo-code, where E is the particle number in the swarm. Pseudocode PSO:

Random initialization of the positions and speeds for each particle
while the stopping criteria aren't reached, do
for i =1 to E do
Displacement of the particle using eq. (1) and (2)
Evaluate the fitness of the swarm
Update p
if $f(x_i) < f(p_i)$ then
$p_i = x_i$
end
Update g
if $f(p_i) < f(g)$ then
$g = p_i$
end
end
end

The stopping criterion may be different depending on the problem posed. If the global optimum is known a priori, we can define an acceptable error as a stopping criterion. Otherwise, it is common to set a maximum number of evaluations of the objective function or a maximum number of iterations, such as the stop criterion. The design of both machines is optimized in terms of mass torque by using particle swarm optimization (PSO) combined with the finite element method (FEM).

3. DESIGN PROCEDURE OF INNER AND OUTER ROTOR FRPM

The following equation allows many combinations between the number of phase q, the number of stator plots N_{ps}, the total number of permanent magnet pairs Ns in the stator, and the number of rotor teeth N_r:

$$\begin{cases} K = \frac{N_r}{N_{ps}} \pm \frac{1}{q} \\ N_{dp}\ max\ i\ mum = K \\ N_{ps} = \frac{N_s}{N_{dp}} \end{cases} \quad (6)$$

The coefficient K is the maximum number of magnet pairs per plot N_{dp}. Both machines have 48 permanent magnets spread over 12 stator plots and 64 teeth in the passive rotor. The overall geometric parameters to be optimized (Fig. 2) are:

- Rotor and stator yokes width E_r and E_s, respectively.
- Coil height h_b.
- Angular plot opening β.
- Point A (R_A, β_A) with R_A and β_A are point A's radius and opening angle.
- Rotor teeth parameters h_r, α_{r1}, and α_{r2}.
- Magnet height h_m.

Like the switched reluctance machine (SRM) with toothed plots, the flux reversal machine (FRM) substitutes alternating permanent magnets for the stator plots' teeth. Its winding is concentric, with two alternating magnets in the stator corresponding to the rotor tooth pitch. In one phase, L's self-inductance is nearly constant. The flux resulting from the current Ψ_w and the flux from the magnets Ψ_{pm} together comprise the total flux Ψ of the FRM (Fig. 3).

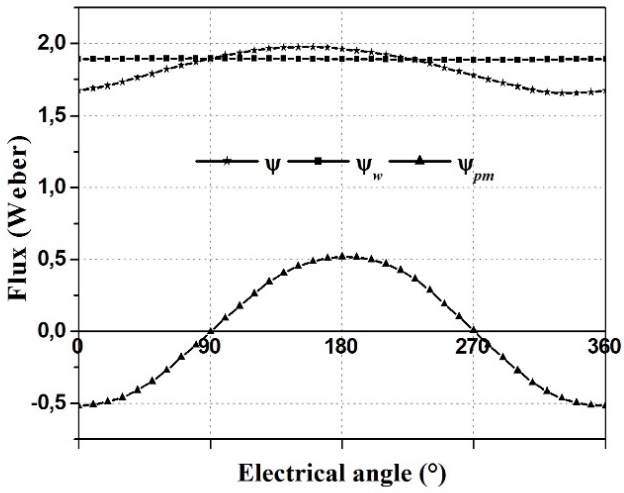

Fig. 3 – Flux versus rotor position.

The distribution of magnetic induction is observed along a contour situated in the center of the air gap, which delimits a whole pad over a 30° mechanical opening when a nominal current is introduced into phase A for the conjunction and opposite positions (Fig. 4 and 5). Without demagnetizing the magnets, the phase A flux reduces the flux of magnets magnetized in the opposite direction and increases the magnets' magnetic flux in the same direction.

For a given phase, the magnetic torque is [10]:

$$T_e = \frac{1}{2} i^2 \frac{dL}{d\theta} + i \frac{d\psi_{pm}}{d\theta} \quad (7)$$

For every rotor position, the integral along a closed contour Γ that surrounds the rotor and is situated in the air gap is determined in two dimensions using the finite elements method:

$$T_e = L \oint_{\Gamma} r H_t B_n \mathrm{d}\Gamma, \quad (8)$$

with L denoting the machine's length, B_n and H_t are the radial and tangential components of the magnetic induction and magnetic field. The power factor of the study FRM is computed using the energy ratio outlined by Lawrenson [19] for a pure switched reluctance machine (SRM):

$$Fp = \frac{W\prime(\theta_{conj}) - W\prime(\theta_{opp})}{[W\prime(\theta_{conj}) - W\prime(\theta_{opp})] + [W(\theta_{conj}) - W_{pm}(\theta_{conj})]}, \quad (9)$$

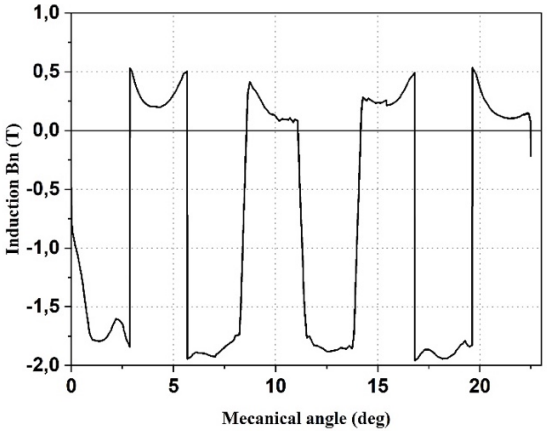

Fig. 4 – Spatial distribution magnetic induction in the middle of the air gap I = In, Phase A in conjunction position.

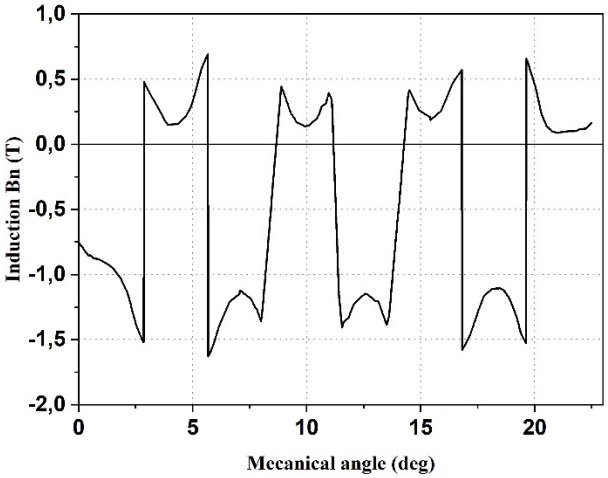

Fig. 5 – Spatial distribution of the magnetic induction in the middle of the air gap I=In, Phase A in opposite position.

where $[W(\theta_{conj}) - W(\theta_{opp})] + [W(\theta_{conj}) - W_{pm}(\theta_{conj})]$ is the energy between the machine and the converter (Fig. 6).

This ratio, comparable to the power factor, evaluates the FRM's energy conversion efficiency. It displays the percentage of energy (W') converted between the machine's and the converter's total energy (co-energy).

The converter's size decreases as this ratio gets better. The energy ratio is improved when permanent magnets are present. For the optimization of the machine's geometry, the objective is to minimize the following function:

$$f = \left(\frac{T}{m}\right)^{-1}, \quad (10)$$

with T is the maximum torque developed by the machine. This torque is obtained for electrical angles close to 90° (Fig. 7) and m, the mass of the active materials, namely iron, copper, and permanent magnets.

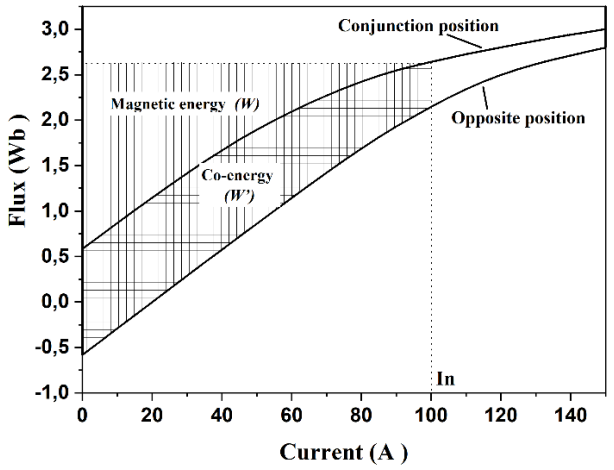

Fig. 6 – FRM energy cycle.

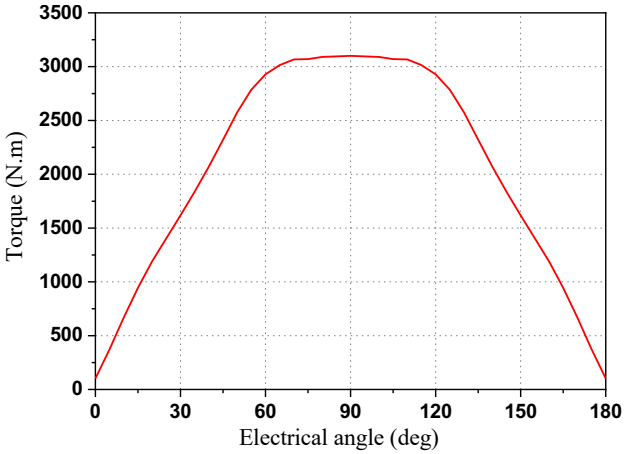

Fig. 7 – Electromagnetic torque versus rotor position

As a result of analytical pre-sizing, the FRM research space at optimization is shown in Table 1, where R_0 is the radius exterior of the machine fixed by the specifications [10] (Table 2):

Table 1

Parameter validity interval

Geometric parameters	Max	Min
R_a (mm)	$R_0/3$	$0.9\times R_0$
E_s (mm)	5	50
β_a (°)	1	15
β (°)	1	15
h_m (mm)	0.2	30
h_b (mm)	5	100
h_r (mm)	0.2	30
E_r (mm)	5	50
α_{r1}	0.2	0.5
α_{r2}	0.2	0.5

Table 2

Design requirements.

Parameters	Values (Units)
Rated power	10 kW
Rated torque	2000 Nm
Outer diameter ($2\times R_0$)	600 mm
Current density	5 A/ mm^2
Coefficient of copper filling	0.5
Air gap thickness	0.5 mm

3. RESULT AND DISCUSSION

Both machines previously described have been designed using the finite element method magnetics (FEMM) software. The PSO is combined with this software (FEMM) for their optimizations. The mass torque (equation 10) is the objective function to optimize. Both machines are intended for generator operation and are dedicated to the wind turbine. For a better comparison, both machines are subjected to the same load specification (Table 2). The other geometrical parameters are delimited in validation intervals, as shown in Table 1.

Figure 8 depicts the convergence of the objective function (mass torque) as a function of generations. It should be noted that:

- At the start of the generations, IRFRPM produces more mass torque than ORFRPM.
- The mass torques of the two machines are nearly identical in the twentieth generation.
- Since then, IRFRPM has stagnated, whereas ORFRPM has continued to advance.
- Finally, IRFRPM achieves its global optimum at the thirty-ninth generation, whereas ORFRPM achieves it at the thirty-seventh generation.

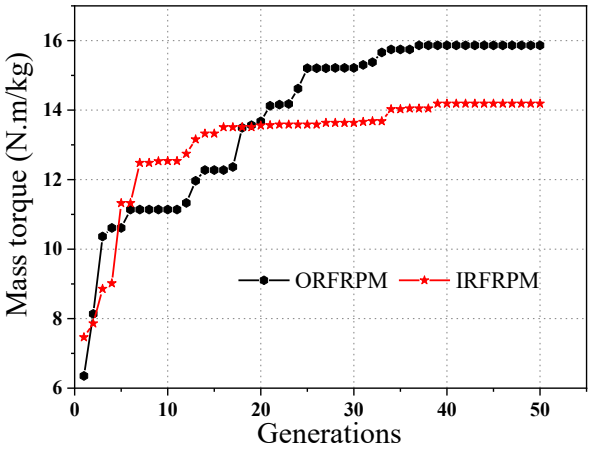

Fig. 8 – Mass torque versus generations.

Figure 9 compares the no-load flux linkage of both machines. Both have a symmetrical flux waveform, but ORFRPM has a larger peak value for the flux link than IRFRPM. The amplitude of the back FEM shown in the figures below confirms this.

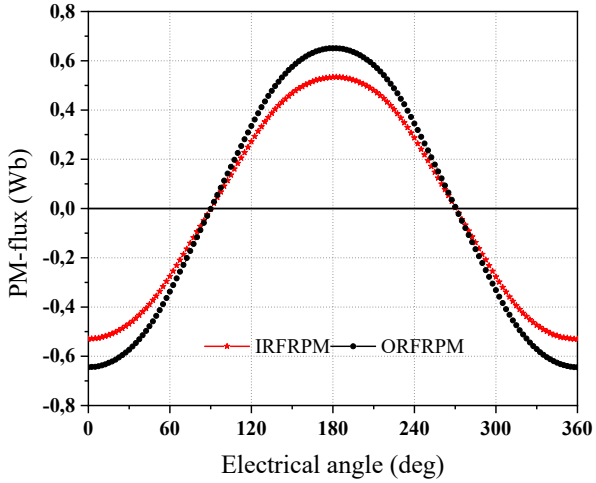

Fig. 9 – Flux linkage.

Figures 10 and 11 show the variation of the two generators' electromotive forces (EMFs) and the corresponding FFT analysis. Given that the number of turns per phase for both machines is 160 (40 turns/plot), the FEM of the ORFRPM (220 V) is greater than that of the IRFRPM (180 V). The ORFRPM improves the induced voltage by 22 %.

Figure 11 also shows an improvement in the second harmonic of ORFRPM. It accounts for 0.47 percent of the fundamental and 1.78 percent of the IRFRPM's second harmonic. Figure 10 demonstrates this, as we can see that ORFRPM has a better EMF waveform than IRFRPM.

Figure 12 shows the cogging torque of the two optimized machines. Table 2 shows that it is minus 10 % of the rated torque fixed by the specifications.

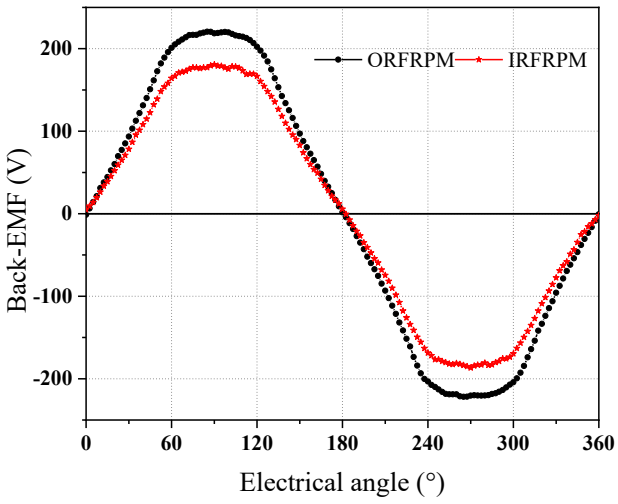

Fig. 10 – Back EMF.

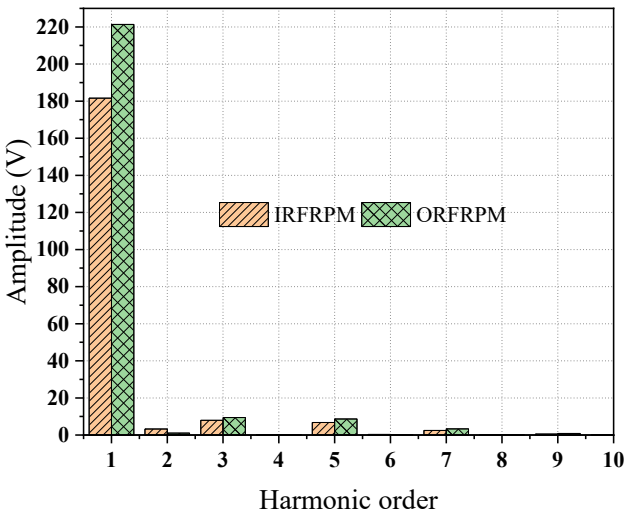

Fig. 11 – FFT analysis of back EMF.

Figure 13 depicts the maximum torque produced by the two machines at various supply currents. Both machines produce nearly the same torque at low currents (I<30 A). However, starting at 60 A, ORFRPM produces more torque than IRFRPM. For example, the torque of ORFRPM is 25% greater than that of IRFRPM for a current of I=90 A

Figure 14 depicts a merged view of the optimized ORFRPM with PSO: (a) design/properties, (b) FEA mesh, (c) flux lines, (d) flux density distribution, and the flux density legend is depicted in the middle of the figure. We notice saturation at the tips of the rotor teeth and the stator plot corners (1.9 T). This is due to the flux's concentration in these narrow regions. In other

regions, such as the stator and rotor yokes and the stator plots, the flux density does not exceed 1.2 T.

Table 3 displays both machines' optimal geometrical parameters, mass torque, maximum torque, total mass, and maximum power. Although the IRFRPM has 17.23 % less mass than the ORFRPM, this is more than offset by the maximum torque (35 %). The ORFRPM's mass torque (+11.76 %) and maximum power (+35.1 %) support this compensation.

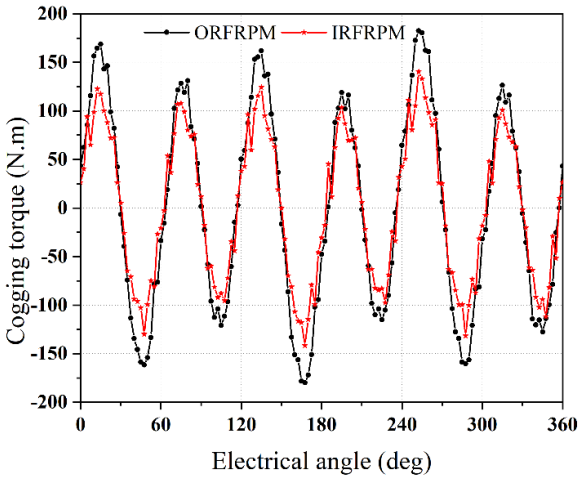

Fig. 12 – Cogging torque.

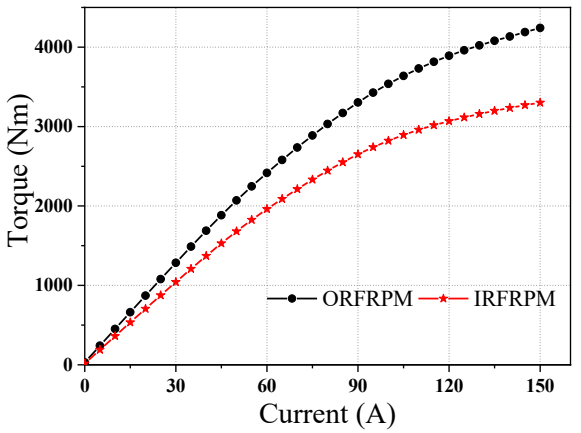

Fig. 13 – Torque versus current.

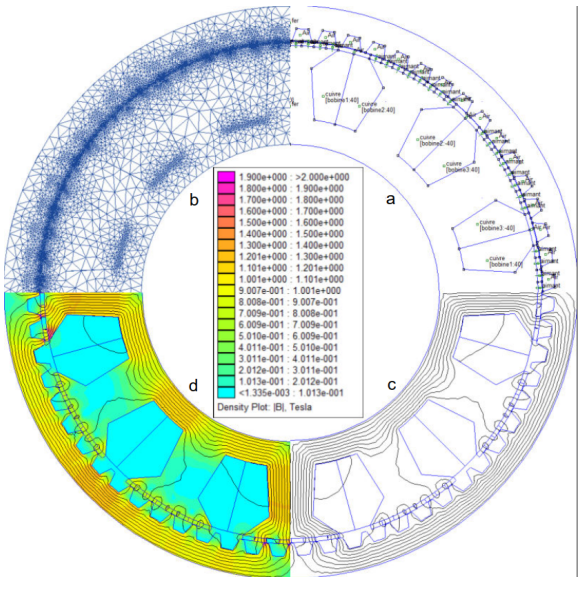

Fig. 14 – Optimized ORFRPM.

Table 3

Parameters of the optimal structures

Parameter	IRFRPM	ORFRPM
Maximum power (kW)	16.04	21.67
Mass torque (Nm / kg)	14.19	15.86
Maximum torque (N.m)	3063.70	4138.77
Total mass (kg)	215.94	260.90
Iron mass (kg)	168.72	204.92
PM mass (kg)	6.26	7.88
Coils mass (kg)	41	48
Geometric parameters		
R_a (mm)	247.15	235.52
E_s (mm)	22.95	27.06
E_r (mm)	23.52	24.21
β_a (°)	4.79	5.56
β (°)	4.75	8.00
h_b (mm)	47.30	75.54
h_m (mm)	3.94	4.34
h_r (mm)	16.20	12.80
α_{r1}	0.20	0.20
α_{r2}	0.44	0.46

5. CONCLUSIONS

The primary goal of this manuscript is to improve a new design: the Outer rotor flux reversal permanent magnet machine. ORFRPM has a better attitude toward direct-drive wind systems than its counterpart IRFRPM. The results presented in this paper support this. ORFRPM is highly desired/recommended for direct-drive wind turbines because it has a largely satisfactory mass torque, an EMF with improved amplitude and waveform, and a good peak torque that directly reflects the machine's average torque. Future work and prospects include investigating the performance of this promising machine (ORFRPM) in a dynamic regime to understand it better and further validate these electromagnetic properties.

Received on 6 June 2023

REFERENCES

1. R.P. Deodhar, S. Andersson, I. Boldea T.J. Miller, *The flux-reversal machine: A new brushless doubly-salient permanent-magnet machine.* IEEE Transactions on Industry Applications, **33,** *4,* pp. 925–934 (1997).
2. I. Boldea, J. Zhang, S.A. Nasar, *Theoretical characterization of flux reversal machine in low-speed servo drives-the pole-PM configuration*. IEEE Transactions on Industry Applications, **38,** *6,* pp. 1549–1557 (2002).
3. T.H. Kim, J. Lee, *A study of the design for the flux reversal machine*. IEEE Transactions on Magnetics, **40,** *4,* pp. 2053–2055 (2004).
4. I. Boldea, C. Wang, S.A. Nasar, *Design of a three-phase flux reversal machine.* Electric Machines &Power Systems, **27,** *8,* pp. 849–863 (1999).
5. C. Wang, S. A. Nasar, I. Boldea, *Three-phase flux reversal machine (FRM).* IEE Proceedings-Electric Power Applications, **146**, *2,* pp. 139–146 (1999).
6. D. S. More, B. G. Fernandes, *Analysis of flux-reversal machine based on fictitious electrical gear,* IEEE Transactions on Energy Conversion, **25,** *4,* pp. 940–947 (2010).
7. C. X Wang, I. Boldea, S. A. Nasar, *Characterization of three phase flux reversal machine as an automotive generator.* IEEE Transactions on Energy Conversion, **16,** *1,* pp. 74–80 (2001).
8. Y. Gao, D. Li, R. Qu, X. Fan, J. Li, H. Ding, *A novel hybrid excitation flux reversal machine for electric vehicle propulsion.* IEEE Transactions on Vehicular Technology, **67,** *1,* pp. 171–182 (2017).
9. D. Li, Y. Gao, R. Qu, J. Li, Y. Huo, H. Ding, *Design and analysis of a flux reversal machine with evenly distributed permanent magnets.* IEEE Transactions on Industry Applications, **54,** *1,* pp. 172–183 (2017).

10. R. Saou, M.E. Zaïm, K. Alitouche, *Optimal Designs and Comparison of the Doubly Salient Permanent Magnet Machine and Flux-reversal Machine in Low-speed Applications*, Electric Power Components and Systems, **36***, 09*, pp. 914–931 (2008).
11. C. Guerroudj, R. Saou, A. Boulayoune, M.E. Zaïm, L. Moreau, *Performance analysis of Vernier slotted doubly salient permanent magnet generator for wind power*. International Journal of Hydrogen Energy, **42,** *13*, pp. 8744–8755 (2017).
12. A. Boulayoune, C. Guerroudj, R. Saou, L. Moreau, M.E. Zaim, *Optimisation par essaim de particule et algorithme génétique d'une machine à inversion de flux*. Revue Roumaine des Sciences Techniques, Série Électrotechnique et Énergétique, **62**, *1*, pp. 19–24 (2017).
13. J. Ojeda, M.G. Simões, G. Li, M. Gabsi. *Design of a flux-switching electrical generator for wind turbine systems*. IEEE Transactions on Industry Applications, 48, 6, pp.1808–1816 (2012).
14. D.S. More, H. Kalluru, B.G. Fernandes, *Outer rotor flux reversal machine for rooftop wind generator*. In 2008 IEEE Industry Applications Society Annual Meeting, Edmonton, Alta, pp. 1–6, 2008.
15. R. Eberhart, J. Kennedy, *A new optimizer using particle swarm theory*. In Proceedings of the Sixth International Symposium on Micro Machine and Human Science, **1**, pp. 39–43. New York, NY, 1995.
16. M. Clerc, J. Kennedy, *The particle swarm — explosion, stability, and convergence in a multidimensional complex space*. IEEE Transactions on Evolutionary Computation, **6**, *1*, pp. 58–73 (2002).
17. P.J. Angeline. *Using Selection to Improve Particle Swarm Optimization.* IEEE International Conference on Evolutionary Computation Proceedings. IEEE World Congress on Computational Intelligence, **89**, pp. 84–89 (1998).
18. Y. Shi, R. Eberhart. *A modified particle swarm optimizer*. In Evolutionary Computation Proceedings, IEEE World Congress on Computational Intelligence., IEEE International Conference on, pap. 69–73 (1998).
19. P.J. Lawrenson, J.M. Stephenson, P. Blenkinsop, J. Corda, N.N. Fulton, *Variable-speed switched reluctance motors*. In IEE Proceedings B-Electric Power Applications, **127,** *4,* pp. 253–265 (1980, July).